BIOCHEMISTRY
including biophysical chemistry & molecular biology

Article

pubs.acs.org/biochemistry

Thermal Inactivation of Uricase (Urate Oxidase): Mechanism and Effects of Additives

Michael S. Caves,*[,†] Barry K. Derham,[‡] Jan Jezek,[‡] and Robert B. Freedman[†]

[†]School of Life Sciences, University of Warwick, Coventry CV4 7AL, U.K.

[‡]Arecor Limited, 2 Cambridge Science Park, Cambridge CB4 0FE, U.K.

Supporting Information

ABSTRACT: Uricase (Urc) is an oxidoreductase enzyme of both general and commercial interest, the former because of its lack of a cofactor and the latter because of its use in the treatment of hyperuricemic disorders. Results of fluorometry and circular dichroism (CD) spectroscopy indicate that the main phase of thermal Urc inactivation follows an irreversible two-state mechanism, with loss of ~20% of the helical structure, loss of the majority of the tertiary structure, and partial exposure of tryptophan residues to solution being approximately concurrent with activity loss. Results of size exclusion chromatography and 8-anilinonaphthalene-1-sulfonate binding studies confirm that this process results in the formation of aggregated molten globules. In addition to this process, CD studies indicate the presence of a rapid reversible denaturation phase that is not completely coupled to the main phase. Urc inactivation is inhibited by the presence of glycerol and trimethylamine oxide, stabilizers of hydrophobic interactions and backbone structure respectively, confirming that loss of hydrophobic bonding and loss of helical structure are key events in the loss of Urc activity. NaCl, however, destabilizes the enzyme at elevated temperature, emphasizing the importance of ionic interactions to Urc stability. A model is developed in which interfacial disruption, involving local loss of hydrophobic interactions, ionic bonds, and helical structure, leads to Urc inactivation and aggregation. Additional studies of Urc inactivation at a more ambient temperature indicate that the inactivation process followed under such conditions is different from that followed at higher temperatures, highlighting the limitations of high-temperature enzyme stability studies.

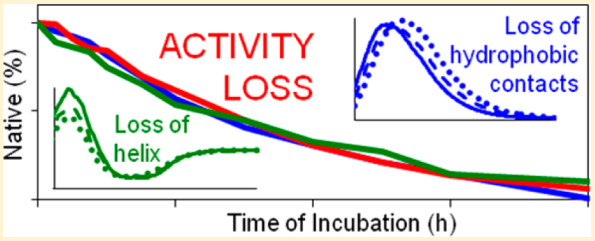

Since it was first isolated in a purified form more than a century ago,[1] urate oxidase, or uricase (Urc), has been the subject of much research, mainly because of its therapeutic and diagnostic applications. Urc catalyzes the oxidation of uric acid into the more soluble allantoin[2] and has found application in therapy, for more than 30 years, in lowering uric acid levels in cancer patients with chemotherapy-induced hyperuricemia.[3] More recently, the enzyme has begun to be used to reduce urate levels in gout patients.[4−7] In relation to diagnosis, the enzyme is used in uricemic disorders, being used to measure serum uric acid concentration,[8,9] and much research into the immobilization of the enzyme for the purpose of biosensor development has been conducted.[10−14] Such applications have inspired research into stabilizing the enzyme through both modification[15,16] and formulation with polyethylene glycol.[17] KRYSTEXXA (formerly known as Puricase), from Savient Pharmaceuticals, Inc., is an example of a commercially available Pegylated Urc pharmaceutical.[5]

Urc is an unusual oxidoreductase enzyme, in that it lacks a cofactor.[18,19] The native enzyme is a globular tetramer with a monomer mass of approximately 32 kDa and a molecular mass of ~130 kDa.[20,21] The native tetramer has an external size of 50 Å × 50 Å.[19,22] Each monomer is composed of two domains, each domain consisting of an antiparallel β-sheet of four sequential strands and a pair of antiparallel helices. The integration of the two topologically identical domains produces a folded monomer consisting of an antiparallel β-sheet of eight sequential strands, with the helices layered on the concave side of the sheet.[19] Therefore, each dimer consists of a β-barrel of 16 sequential antiparallel strands, with the eight helices forming the exterior of the barrel. The folded Urc tetramer contains four active sites, located at the dimerization interfaces, and the dimers stack in a face-to-face manner in the tetramer, giving a tunnel 50 Å long and 12 Å in diameter.[19,22]

In this paper, we analyze the kinetics and mechanism of Urc inactivation in aqueous solution at moderately elevated temperatures and the effects of some well-known additives [NaCl, glycerol, and trimethylamine oxide (TMAO)] on this process. To the best of our knowledge, this work represents the first biophysical study of the inactivation mechanism of Urc, and the results shed new light both on the structural changes that occur during Urc inactivation and on factors affecting the reversibility of the process. Our analysis contributes to the general study of protein denaturation, especially considering the unique status of Urc as a cofactor-free oxidoreductase, and also

Received: September 30, 2012
Revised: December 9, 2012
Published: December 13, 2012

   dx.doi.org/10.1021/bi301334w | *Biochemistry* 2013, 52, 497−507

provides information important to the practical applications of Urc as a pharmaceutical and diagnostic agent.

EXPERIMENTAL PROCEDURES

Purification. A commercial preparation of urate oxidase (EC 1.7.3.3) from *Candida* sp. (expressed in *Escherichia coli*) (Sigma-Aldrich) was purified using a xanthine-agarose affinity chromatography method similar to that detailed previously.[15] Xanthine-agarose (Sigma-Aldrich) was equilibrated with 10 column volumes of 50 mM borate buffer (pH 8.5) before the application of impure Urc, dissolved in 50 mM borate buffer (pH 8.5), to the column. The unbound fraction was removed with 20 column volumes of 50 mM borate buffer (pH 8.5). The enzyme was then specifically eluted from the column with 5 column volumes of 1.2 mM uric acid in 20 mM borate buffer (pH 8.5).

Inactivation of Urc for Steady State Studies. Solutions of Urc were incubated in a Grant (Cambridge, U.K.) GR150 precision stirred thermostatic bath at the required temperature and pH. Aliquots were removed at specific time points and refrigerated immediately. The residual activity of Urc was then measured in the samples no longer than 48 h after the refrigeration.

Activity Assays. Urc activity was assayed at 25 °C using the following method. The sample, 10 μL (diluted in borate buffer to a Urc concentration of 360−720 nM), was added to a cuvette containing 1490 μL of the assay mixture [consisting of 125 μM uric acid in 0.1 M borate buffer (pH 8.5)]. A Cary 100 spectrophotometer (Varian) was used to measure the absorbance at 293 nm at 0.25 min intervals for 5 min after addition of the sample to the assay mixture. For each set of assays, a number of standards of known Urc concentration were also assayed. The resulting calibration curve was consistently linear with an R^2 value of >0.99. Where specific activity is quoted, 1 unit is defined as the amount of enzyme that catalyzed the oxidation of 1 μmol of uric acid per minute at pH 8.5 and 25 °C.

CD Measurements. CD scans were performed on a Jasco J-815 CD spectropolarimeter. A bandwidth of 1 nm, a data pitch of 0.5 nm, and a response time of 1 s were used for all scans. All spectra presented here are the average of 16 consecutive scans. Far-UV CD scans in the range of 260−185 nm were performed using a 1 mm path length cuvette, and near-UV CD scans in the range of 320−240 nm were performed using a 10 mm path length cuvette.

For continuous monitoring of the change in CD during inactivation, 0.1 M borate buffer (pH 10.0) (in the appropriate cuvette) was heated to the required temperature in the CD spectrometer cell. The temperature of the cell was maintained with a Jasco PFD-4255/15 Peltier block. To start inactivation, an aliquot of enzyme sample, at a concentration 10 times the final concentration in the same buffer, was diluted 1/10 in the buffer in the cuvette (see the figure legend for the final concentration). This allowed rapid heating of the enzyme to the required temperature. Monitoring by the spectropolarimeter was initiated before the Urc was added to the cell, and the moment that the spectropolarimeter cell lid was closed was taken as time zero.

Fluorescence Measurements. Fluorescence scans were taken with a Photon Technology International fluorometer. An excitation and emission bandwidth of 2 nm and a response time of 1 s were used for all scans. Emission spectra of tryptophan residues were observed upon excitation at 295 nm, using a data pitch of 0.5 nm. Binding of the external chromophore, ANS, to Urc was assessed using an excitation wavelength of 390 nm and a data pitch of 1 nm. All fluorescence measurements were performed using a 5 mm × 5 mm square cuvette. All spectra presented here are the average of four consecutive scans and are expressed as relative fluorescence intensity (RFI).

Size Exclusion Chromatography. SEC measurements were taken using a Superdex 200 column (10 mm × 300 mm, GE Healthcare) on an AKTA purifier system (GE Healthcare). An injection volume of 470−500 μL and a flow rate of 0.5 mL/min were used, with a protein concentration of 6.1−7.1 μM. Samples were eluted isocratically using a 0.1 M borate buffer (pH 10.0) mobile phase. Detection was conducted at 280 nm. The column was calibrated with markers of known molecular mass, namely, cytochrome *c*, carbonic anhydrase, bovine serum albumin, alcohol dehydrogenase, and β-amylase, with blue dextran being used as a void volume marker.

Data Processing. Curve fitting was performed using SigmaPlot 9.0. Secondary structure prediction from CD data was performed using the online Dichroweb application.[23] The CDSSTR SVD analysis method[24] was used with Reference data set 6.[25]

Data are presented with error bars whose lengths represent one standard deviation either side of the mean. Unless otherwise stated, activity data are normalized using the activity of the untreated enzyme as the maximum. Where appropriate, activity, fluorescence, and CD data were normalized using the following equation:

$$X = [(P_\alpha - P_t)/(P_\alpha - P_0)] \times 100 \quad (1)$$

where X is the residual enzyme (percent) with the native parameter at time t, P_α is the final parameter value, P_t is the parameter value at time t, and P_0 is the parameter value at time zero. CD raw data were converted (from millidegrees) to mean residue ellipticity (MRE) using the following equation:[26]

$$[\theta]_{\mathrm{MRW},\lambda} = (\mathrm{MRW} \times \theta_\lambda)/(10dc) \quad (2)$$

where $[\theta]_{\mathrm{MRW},\lambda}$ is the mean residue ellipticity at wavelength λ (degrees square centimeters per decimole), MRW is the mean residue weight (daltons), θ_λ is the observed ellipticity (millidegrees), d is the path length (centimeters), and c is the Urc concentration (milligrams per milliliter). A mean residue weight of 113 Da was used.

RESULTS

Purification and Characterization of Urc and Initial Analysis of Inactivation. Xanthine-agarose affinity chromatography removed significant impurities from the commercial *Candida* sp. Urc preparation, and the resultant material was shown to be relatively homogeneous by sodium dodecyl sulfate−polyacrylamide gel electrophoresis (SDS−PAGE) (Figure S1A of the Supporting Information). The purified sample resolves a single intense band slightly below 36 kDa (the UniProt database lists Urc monomers from *Candida utilis* as having a molecular mass of 34 kDa), with another much fainter band slightly above 36 kDa. The relative intensities of the bands were not altered by affinity chromatography, suggesting that both bands consist of material with similar xanthine binding properties. Mass spectrometry analysis of peptide digests confirmed that both bands consist of Urc monomers (data not shown).

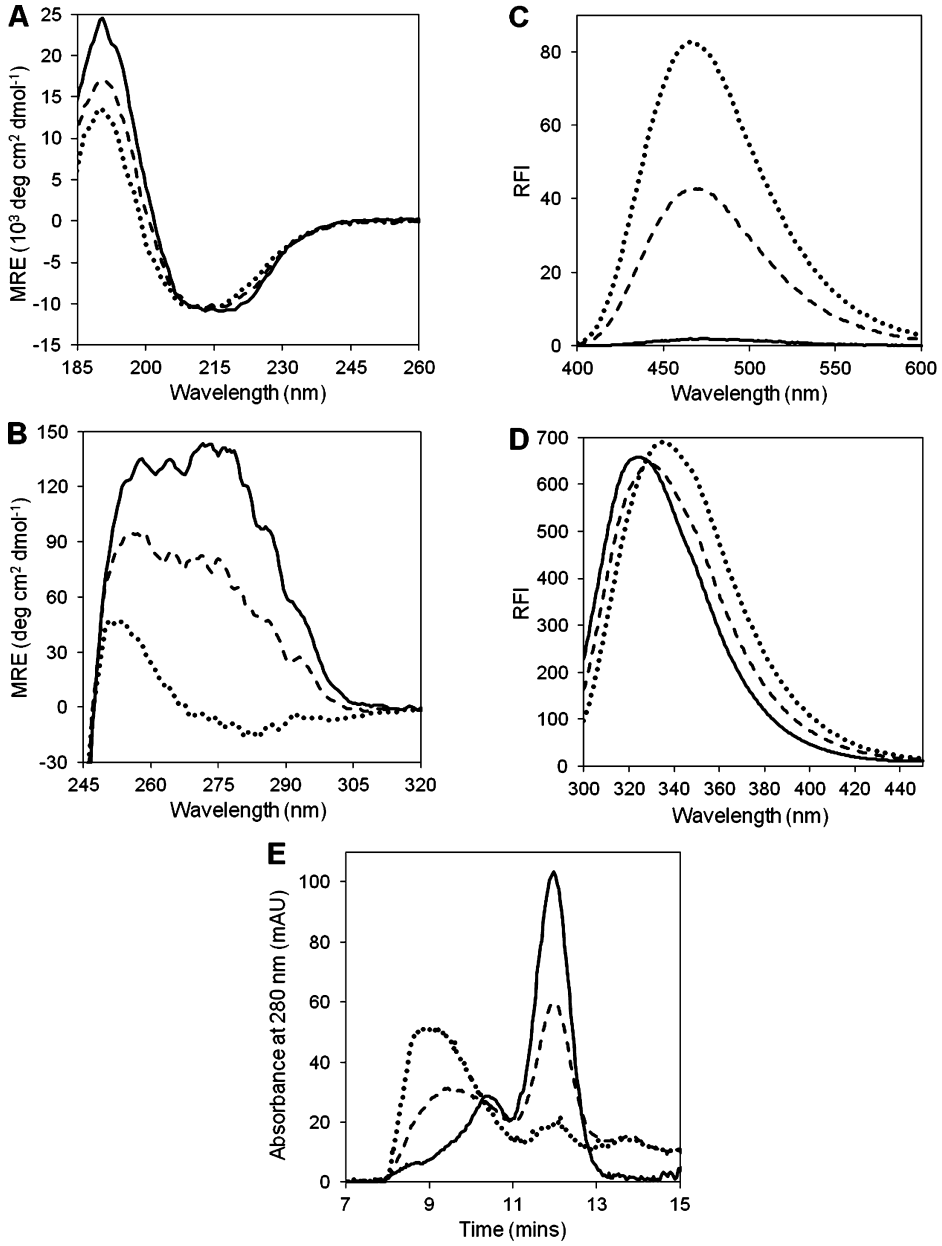

Figure 1. Formation of the aggregated molten globule upon inactivation. Steady state CD, fluorescence, and SEC measurements of Urc of different activities after incubation at a concentration of 7.1 μM for various times at 57.5 °C in 100 mM borate buffer (pH 10.0): (—) 100% active, (– – –) ~50% active, and (···) <10% active. (A) Far-UV CD scans using 0.71 μM Urc in 10 mM borate buffer (pH 10.0) after 1/10 dilution of samples in deionized water. (B) Near-UV CD scans using 7.1 μM Urc in 100 mM borate buffer (pH 10.0). (C) ANS fluorescence emission scans using 1.4 μM Urc and 250 μM ANS, in buffer as for panel B, with an excitation wavelength of 390 nm. (D) Trp fluorescence emission scan using the same Urc concentration and buffer as in panel B, with an excitation wavelength of 295 nm. (E) SEC measurements using an injection Urc concentration of 7.1 μM and an injection volume of 500 μL.

The purified Urc was also analyzed by size exclusion chromatography (Figure S1B of the Supporting Information), which showed a major peak at 12.0 mL (>70% of the material) that corresponded to the native Urc tetramer. There was additionally a peak with an elution time of 10.4 mL representing an entity with a molecular mass of 260 kDa (roughly corresponding to a Urc octamer), along with some higher-mass species with an elution volume of <10.4 mL. Reducing SDS–PAGE on all fractions from this SEC profile gave a pattern identical to that observed for purified Urc (Figure S1A of the Supporting Information), so that all the material comprised oligomers of the same Urc polypeptides (data not shown).

It has been reported previously that one of the three Cys residues present in each monomer is surface-accessible to 5,5′-dithiobis(2-nitrobenzoic acid) (DTNB) in the folded protein[18] and that, in the absence of a reducing agent, Urc tends to polymerize, producing a slight loss of enzyme activity. Figure S1B of the Supporting Information also shows the SEC profile of Urc in the presence of 20 mM DTT, indicating that the reducing agent reduces considerably the level of higher oligomers in the Urc preparation. This is consistent with the 10.4 mL peak consisting of Urc tetramers disulfide-bonded

dx.doi.org/10.1021/bi301334w | *Biochemistry* 2013, 52, 497–507

together to form octamers and with the material that elutes at elution volume(s) of <10.4 mL also consisting of higher Urc oligomers bound together by disulfide linkages.

We compared the specific activities of Urc with and without inclusion of 2 mM DTT in the assay buffer. These assays (performed in triplicate) demonstrated that DTT treatment leads to an insignificant change in specific activity (<1%) (data not shown). The lack of any significant increase in activity upon reduction is consistent with the observed oligomers being composed of native, fully active Urc tetramers bound together by disulfide bridges. For this reason, we did not routinely conduct further analyses in the presence of DTT.

Preliminary work indicated that the stability of Urc at an elevated temperature declined as the pH of the solution was increased from 8 to 10 (Figure S2A of the Supporting Information). Studies conducted at pH 7 demonstrated that the enzyme is less stable at this pH than at pH 8 (data not shown), indicating that the pH of optimal stability for Urc is ∼8. The protein absorbance data in Figure S2B of the Supporting Information indicate that Urc precipitates from solution upon inactivation at pH 8 and also to some extent at pH 9, but that this effect is minimized by incubation in pH 10 buffer. For this reason, pH 10 was used for all further studies and the rate of inactivation was controlled by varying the temperature applied. Incubation of Urc in pH 10 borate buffer at a temperature of 57.5 °C resulted in loss of >90% of activity within 6 h and gave a convenient rate of inactivation to allow samples of varying activity to be removed at different time points for structural studies. No significant precipitation of Urc from solution was observed after incubation for 8 h under these conditions (data not shown).

Urc Inactivation Leads to the Formation of a Molten Globule and Nonspecific Aggregation. Sampling studies, in which samples were incubated at elevated temperature for set time periods before being cooled and analyzed, were used to assess the major biophysical changes occurring upon Urc inactivation. Far-UV CD spectra of Urc of different activities are shown in Figure 1A. The results demonstrate a small change in secondary structure, with loss of signal at 222 nm and a small red shift in the negative maximum from 217 to 213 nm upon complete inactivation. There is also a significant decrease in the magnitude of the positive signal in the 185−200 nm region. Figure 1A demonstrates that approximately 20% of the initial mean residue ellipticity at 222 nm is lost upon complete inactivation of Urc. This parameter alone can give an estimate of the change in protein helical content,[27] but better quantitation can be achieved by full deconvolution analysis of the spectra in Figure 1A using Dichroweb online software. This indicated that 24% of the native Urc backbone consists of α-helix, a value that decreases to 22% in ∼50% active Urc and 19% upon complete inactivation, confirming a loss of approximately 20% of the initial α-helical content upon inactivation. For comparison, the Protein Data Bank (PDB) contains information about Urc from three different sources (entries 1J2G, 1VAX, and 1R56), the backbone of each variant being estimated to consist of between 23 and 26% α-helix.

Near-UV CD spectra on corresponding samples are shown in Figure 1B. CD in the near-UV range measures asymmetry of aromatic residue environments and is generally taken as a measure of protein tertiary structure.[26] The almost complete loss of ellipticity between 250 and 300 nm is thus indicative of an almost complete loss of Urc tertiary structure during inactivation. The CD signal of Urc at 275 nm changes from 137 to −7 deg cm^2 dmol^{-1} as the activity is reduced from 100 to <10%, though there is some residual signal below 265 nm (Figure 1B). The CD signal between 250 and 265 nm in denatured proteins can be explained by the inherent asymmetry of disulfide bonds[28] and phenylalanine residues.[29]

CD studies therefore demonstrate that Urc loses only ∼20% of its α-helical content but undergoes almost complete loss of tertiary structure upon inactivation. This is consistent with molten globule formation.[30] Figure 1C demonstrates that upon inactivation of Urc there is a significant increase in ANS fluorescence enhancement by the protein, with a peak emission below 500 nm. ANS fluorescence enhancement with an emission peak below 500 nm is a recognized trait of proteins in the molten globule state.[31]

Figure 1D displays the tryptophan fluorescence emission spectra of Urc samples of different activities. As Urc activity declines, there is an 11 nm red shift in the emission maximum, with an initial emission peak of 323.9 ± 0.6 nm, a peak at 329.8 ± 0.4 nm in the 50% active sample, and a peak at 335.0 ± 0.7 nm in the <10% active sample. This is indicative of an increase in the polarity of the environment of the protein's Trp residues upon inactivation.

Figure 1E illustrates the changes in Urc quaternary structure upon inactivation as measured by SEC. The large peak at 12.0 mL corresponds to the native Urc tetramer. As Urc loses activity, a decrease in the proportion of tetramer in the sample is concomitant with an increase in the level of higher-molecular mass species. The ∼50% active sample contains a smaller but still significant amount of tetramer but also contains a wide peak around 9.4 mL. This peak corresponds to a molecular mass of ∼360 kDa, though its width suggests a range of oligomer sizes, indicating that aggregation does not lead to the formation of specific higher-order structures of defined stoichiometry, but to a range of species containing various numbers of denatured Urc molecules. The nonspecific nature of this aggregation is further demonstrated by the shifting of the aggregate peak to higher masses as inactivation proceeds. In the <10% active sample, the aggregate peak is dominant and has shifted to a lower elution volume while the native peak has almost disappeared. The non-Gaussian distribution of the oligomer peak in the <10% active sample can be explained as the effect of large aggregates entering the column void. Using the marker dextran blue, the void volume of the column used was found to be 8.3 mL, corresponding to a molecular mass of >500 kDa. Estimation of the average oligomer size in the <10% active Urc peak is difficult, but the trace indicates that a significant proportion of aggregated species has a molecular mass of >500 kDa.

Comparison of Rates of Change of Several Parameters during Urc Inactivation. Figure 2 shows the normalized changes in activity, CD at 222 nm, and Trp fluorescence maximal emission wavelength, assessed in Urc samples after incubation for varying amounts of time at 57.5 °C, and reveals that changes in these parameters occur concurrently.

To allow more accurate kinetic assessment, real-time studies were used to compare the loss of tertiary structure and secondary structure continuously during Urc inactivation. Samples were incubated in the CD cuvette holding cell at 62.0 °C, and the changes in the signal at 222 and 275 nm were monitored, with a reading taken every second. The number of data points generated during real-time studies also allowed an accurate assessment of the kinetics of Urc inactivation. There was no measurable difference between the rate of change of CD

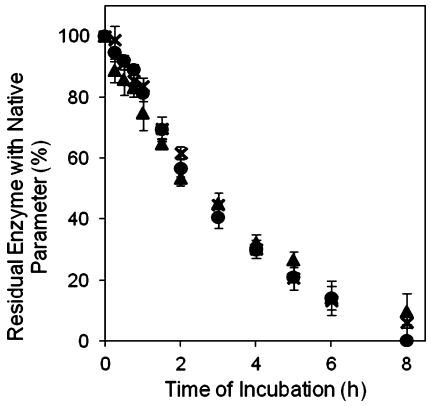

Figure 2. Steady state comparison of changes in various parameters during incubation at elevated temperatures. Measurements taken from steady state scans of Urc after incubation at a concentration of 7.1 μM for various times at 57.5 °C in 100 mM borate buffer (pH 10.0). Each data set is the average of three separate incubations. Data normalized using the native uricase measurements as the maxima and, for fluorescence and CD measurements, the averages of two sets of scans taken for each parameter upon completion of continuously monitored inactivations (Figure 3) were taken as the minima: (×) activity, (●) CD at 222 nm, and (▲) Trp fluorescence wavelength of maximal emission, excitation wavelength of 295 nm.

at 222 and 275 nm assessed by real-time studies (Figure 3), confirming that changes in secondary and tertiary structure are concurrent.

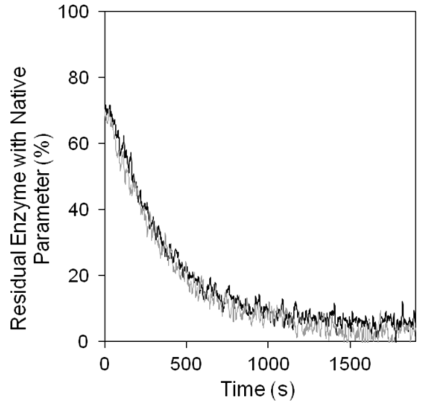

Figure 3. Continuous monitoring of changes in various parameters during incubation at elevated temperatures. Measurements taken in real time during incubation of 7.1 μM uricase in 100 mM borate buffer (pH 10.0) at 62.0 °C. Each data set is the average of two separate incubations. Data normalized using the native uricase measurements as the maxima and the averages of two sets of scans taken for each parameter upon completion of monitoring as the minima: black for tertiary structure and gray for secondary structure.

The data from real-time studies (Figure 3) were fitted adequately to single-exponential fits. Data from duplicate runs indicated that the data at 222 nm were fit by a single first-order rate constant of $(2.75 \pm 0.13) \times 10^{-3}$ s^{-1}, while those at 275 nm were fit by a constant of $(2.94 \pm 0.07) \times 10^{-3}$ s^{-1}. The analyses showed that the exponential process accounted for 71% (at 222 nm) or 72% (at 275 nm) of the observed total change (±2%). In addition to supporting the conclusion that loss of tertiary structure and loss of secondary structure are concurrent events during Urc inactivation, these values also support another observation that can readily be made from Figure 3, that real-time analysis at 62.0 °C allows observation of only ~70% of the total structural change (i.e., the difference between completely inactivated and fresh Urc sample), with the remainder occurring during the experimental dead time. Because the dead time of these experiments was ~5−10 s, the data suggest the presence of an initial rapid phase of uricase denaturation, accounting for ~30% of the total, lasting a matter of seconds at 62.0 °C.

Reversibility of Urc Denaturation. Panels A and B of Figure 4 show the results of continuous monitoring of the CD signal at 222 nm of Urc incubated at 57.5 °C, the same temperature at which the enzyme was incubated for the sampling studies of Figure 2. Figure 4A shows that by the 1800 s time point, ~35% of the overall loss of the CD signal at 222 nm has been completed, in contrast with the <10% of the overall loss of 222 nm ellipticity indicated by the sampling studies. The trace also shows that cooling after 1800 s leads to regeneration (over the following 400 s) of ~20% of the overall signal loss, after which the signal stabilizes at a value similar to that given by the sampling approach. This result indicates that the apparently slow inactivation observed at the early time points in sampling studies (Figure 2) is due to partial refolding of the enzyme upon cooling. Figure 4A also shows multiphasic denaturation, with a phase of rapid change in the CD signal at 222 nm over the initial 60 s of incubation, after which the rate of denaturation slows considerably. This explains the large loss of the CD signal that occurs during the dead time in Figure 3.

Figure 4B indicates that if Urc is incubated for a longer period of time at 57.5 °C the partial refolding capability is lost, and the denaturation becomes completely irreversible. Figure 4C shows the results of a similar continuous analysis of denaturation and reversibility conducted at 62.0 °C. It shows that significant reversibility is possible even upon completion of ~90% of the structural changes that occur during Urc denaturation. The contrast with Figure 4B, which shows that at 57.5 °C reversibility is lost by the time that ~55−65% of the denaturation has occurred, suggests that the loss of reversibility is a function of time spent at the elevated temperature, and not just the degree of denaturation undergone. Near- and far-UV CD measurements indicate that incubation of Urc for >1800 s at 62.0 °C leads to completely irreversible inactivation (data not shown).

Effect of Additives on Urc Stability at Elevated Temperatures. Incubation of Urc at elevated temperatures was performed at various concentrations of NaCl. A lower buffer concentration of 10 mM was used here to minimize the contribution of the buffer to the ionic strength of the composition. Figure 5A shows that NaCl decreases the stability of Urc in a concentration-dependent manner. At 57.5 °C, a half-life of >8 h in the absence of NaCl decreased to ~1.5 h in the presence of 500 mM NaCl. Increasing the incubation temperature to 60.0 °C leads to a decrease in the half-life of Urc activity in the presence of 500 mM NaCl to ~0.75 h (Figure S3 of the Supporting Information), though this 2.5 °C temperature increase has little effect on the stability of Urc in the absence of NaCl.

Figure 5B shows the results of incubation of Urc at 65.0 °C in 10 mM borate buffer (pH 10.0) containing various concentrations of glycerol. Glycerol increases the stability of Urc in a concentration-dependent manner. At 65.0 °C, the half-life of Urc activity incubated in 10 mM borate buffer in the absence of glycerol is 2−3 h, a figure that increases to ~6 h in

dx.doi.org/10.1021/bi301334w | *Biochemistry* 2013, 52, 497−507

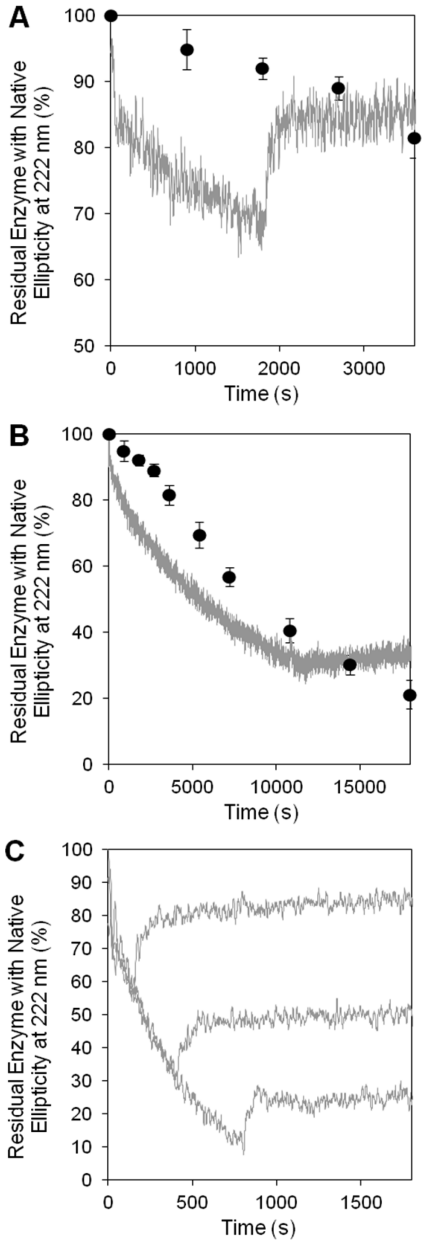

Figure 4. Continuous monitoring of the reversible phase of Urc inactivation at elevated temperatures. CD measurements at 222 nm taken during incubation of 7.1−7.5 μM Urc in 100 mM borate buffer (pH 10.0). All data were normalized using the same method that was used for Figure 3. (A and B) Measurements taken at 57.5 °C. For comparison, corresponding time points from the steady state analysis of the change in the CD signal at 222 nm (Figure 2) are included: (gray line) continuously monitored, average of two sets of data; (●) steady state data (from Figure 2). (A) Cooled to 20.0 °C after 1800 s (0.5 h). (B) Cooled to 20.0 °C after 10800 s (3 h). (C) Measurements taken at 62.0 °C, with samples cooled to 20.0 °C after 150, 400, and 800 s.

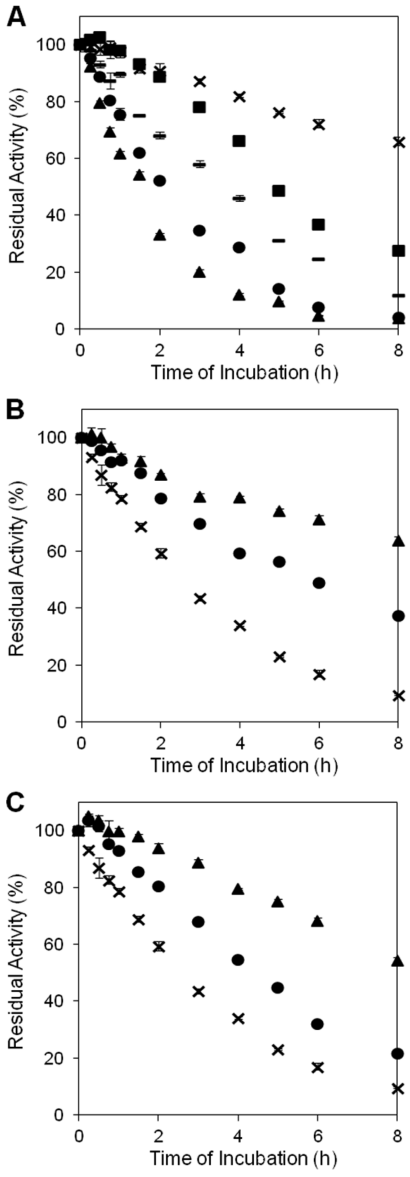

Figure 5. Effect of additive concentration on the rate of Urc inactivation at elevated temperatures. Change in activity over time of 7.1 μM Urc incubated in 10 mM borate buffer (pH 10.0) containing various concentrations of additive. (A) Incubated at 57.5 °C in (×) 0, (■) 50, (−) 100, (●) 200, and (▲) 500 mM NaCl. (B) Incubated at 65.0 °C in (×) 0, (●) 300, and (▲) 1000 mM glycerol. (C) Incubated at 65.0 °C in (×) 0, (●) 900, and (▲) 1800 mM TMAO.

the presence of 300 mM glycerol and >8 h in the presence of 1000 mM glycerol (Figure 5B). The stability conferred upon Urc by the presence of glycerol is also evident at 60.0 °C (Figure S3 of the Supporting Information).

Figure 5C demonstrates that TMAO increases Urc stability in a concentration-dependent manner. The half-life of Urc incubated at 65.0 °C in 900 mM TMAO is 4−5 h. For comparison, the half-life of Urc incubated at the same temperature in 300 mM glycerol is ∼6 h (Figure 5B). This comparison indicates that TMAO is a weaker stabilizer of Urc than glycerol. Data at other concentrations support this conclusion.

CD and fluorescence studies of samples of Urc from various time points of the experiments described in Figure 5A−C showed that the presence of NaCl, glycerol, or TMAO has no differential effect on the changes in the structural parameters (Figure 1A−D) observed in the absence of these additives at elevated temperatures; these additives simply increase (in the case of NaCl) or decrease (in the case of glycerol and TMAO) the rate of the observed changes in far- and near-UV CD and intrinsic and ANS fluorescence (data not shown).

Urc Inactivation under More Ambient Conditions. All results described thus far in this paper were attained at elevated

dx.doi.org/10.1021/bi301334w | *Biochemistry* 2013, 52, 497−507

temperatures, ≥57.5 °C. To assess the inactivation of Urc over longer time periods under more ambient conditions, studies in the absence and presence of NaCl and glycerol were also conducted at 40.0 °C. Figure 6 demonstrates that NaCl is destabilizing at 40.0 °C, just as it is over the temperature range of 57.5−60.0 °C (Figure 5A and Figure S3 of the Supporting Information). However, the magnitude of the effect is much smaller at 40.0 °C, and the concentration dependence is lost. The half-life of Urc at 40.0 °C in the presence of both 150 and 500 mM NaCl is ∼80% of that in the absence of NaCl, with the former being ∼800 h and the latter being ∼1000 h. This contrasts with the results at higher temperatures, where considerable concentration dependence was observed (Figure 5A and Figure S3 of the Supporting Information). Figure 6 also shows that glycerol has a strong, concentration-dependent stabilizing effect on Urc at 40.0 °C, as it does at 60.0−65.0 °C (Figure 5B and Figure S3 of the Supporting Information).

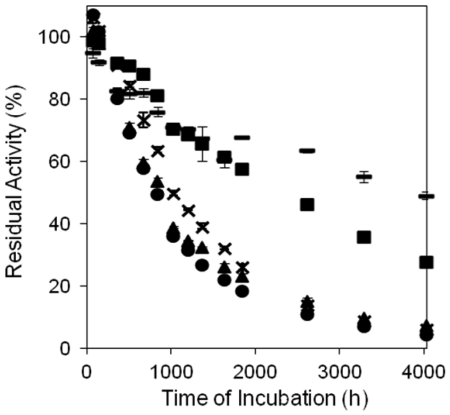

Figure 6. Effect of additive concentration on the rate of Urc inactivation at more ambient temperature. Change in activity of 7.1 μM Urc incubated at 40.0 °C in 10 mM borate buffer (pH 10.0) containing various concentrations of additive: (×) no additives, (■) 300 mM glycerol, (−) 1000 mM glycerol, (●) 150 mM NaCl, and (▲) 500 mM NaCl.

Far- and near-UV CD, intrinsic fluorescence, and fluorescence in the presence of ANS were determined for samples of Urc from various time points in the incubation described in Figure 6. Figure 7A demonstrates that during incubation at both 40 and 65 °C, inactivation of Urc in 1000 mM glycerol involves a red shift in the fluorescence emission of Trp residues, with little change in the fluorescence intensity. Native Urc gives an emission maximum of 324.0 ± 0.4 nm, while a fluorescence emission maximum of 328.1 ± 0.6 nm is observed for Urc with a residual activity of 64 ± 1% after incubation in 1000 mM glycerol at 65.0 °C for 8 h. This is consistent with the results shown in Figure 1D, which demonstrate a red shift of 11 nm upon complete inactivation of Urc. However, the emission maximum of Urc with 49 ± 1% residual activity after incubation for 4032 h in 1000 mM glycerol at 40 °C is 326.1 ± 0.6 nm, red-shifted only 2 nm relative to the native value. Figure 7A, therefore, indicates that the extent of exposure of hydrophobic

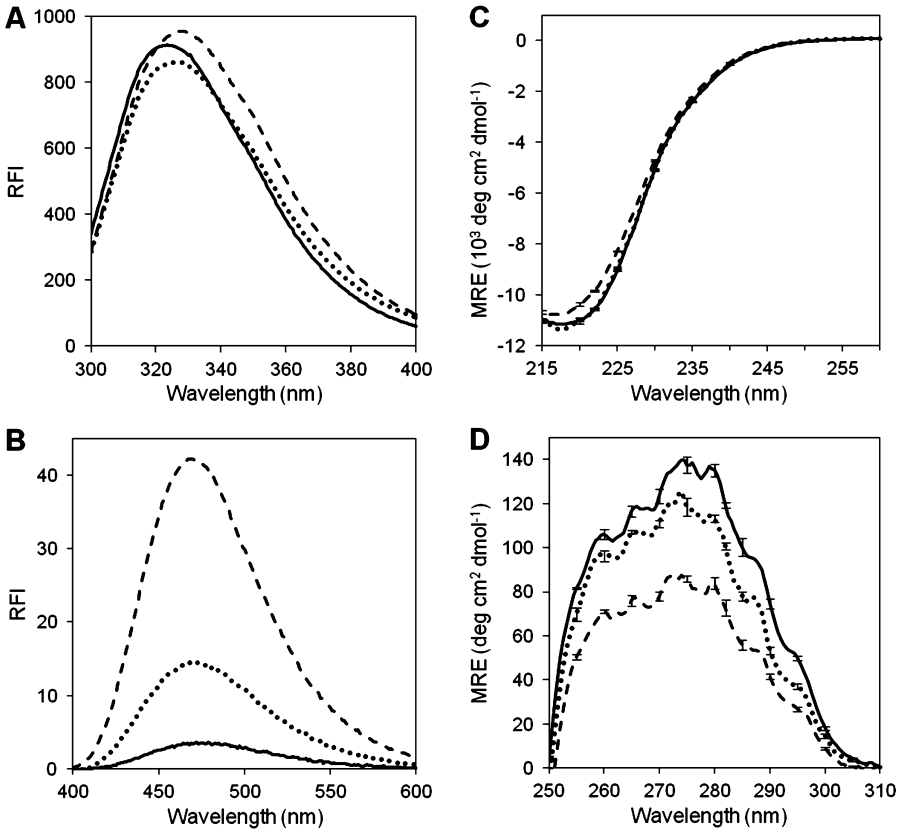

Figure 7. Biophysical changes upon inactivation of Urc in the presence of 1000 mM glycerol at different temperatures. Steady state analysis of 7.1 μM Urc samples after incubation in 10 mM borate buffer (pH 10.0) containing 1000 mM glycerol: (—) 100 ± 1% active, (−−−) 64 ± 1% active after incubation at 65.0 °C for 8 h, and (···) 49 ± 1% active after incubation at 40.0 °C for 4032 h. (A) Trp fluorescence, with an excitation wavelength of 295 nm. (B) ANS fluorescence emission scans using 1.4 μM UrC and 250 μM ANS. (C) Far-UV CD. (D) Near-UV CD.

dx.doi.org/10.1021/bi301334w | *Biochemistry* 2013, 52, 497−507

residues to solution is smaller in the Urc inactivated at the lower temperature, despite the extent of inactivation being greater.

Similarly, panels B–D of Figure 7 show that the extents of ANS fluorescence enhancement, secondary structure loss, and tertiary structure loss are smaller in the Urc incubated at 40.0 °C for 4032 h than in that incubated at 65.0 °C for 8 h, despite the former having undergone a greater degree of activity loss than the latter. Figure 7 indicates, therefore, that the inactivation of Urc in 1000 mM glycerol follows an inactivation mechanism at 40.0 °C different from that followed at 65.0 °C.

DISCUSSION

Structural Basis of Inactivation: Aggregation following Subunit Interface Disruption and Molten Globule Formation. Inactivation of Urc at elevated temperatures produced almost complete loss of tertiary structure, produced retention of ∼80% of α-helical structure, and increased ANS fluorescence consistent with molten globule formation and retention of some of the hydrophobic core.

A red shift in the intrinsic fluorescence upon inactivation showed that Trp residues of Urc undergo an increase in environmental polarity, presumably because of an increase in surface exposure. A plausible explanation for this is that disruption at the subunit interfaces leads to exposure of Trp residues at these interfaces to solution. There is no PDB entry for the crystal structure of *Candida* sp. Urc, but a BLAST comparison of the sequences of Urc from various sources reveals that *Candida* sp. Urc is closely homologous to that from *Aspergillus flavus* with four conserved Trp residues per monomer. The *A. flavus* structure (PDB entry 1R56) shows that two of these are located at the tetramerization interface (between the two dimers), while the others form part of the hydrophobic core of each subunit. The observed Trp fluorescence red shift from 324 to 335 nm is consistent with the Trp residues at the subunit interface becoming solvent-exposed while the more centrally located residues remain relatively buried. This interpretation is consistent with those from studies of pressure-induced Urc inactivation[32] and theoretical work.[33]

We found that the pH of optimal stability of Urc is ∼8, consistent with previous studies of Urc from various sources,[15,34−37] but also observed that inactive Urc at this pH precipitates rapidly. The pI of the enzyme has been found to be 5.4[38] or 5.6.[39] For many proteins, the pH of optimal stability is close to the pI, because of the minimal net protein charge, and minimal intramolecular repulsion, at this pH,[40] but we found that Urc was most stable at a pH of ∼8, >2 pH units above the pI. Figure S4 of the Supporting Information shows that charged residues are unevenly distributed in *A. flavus* Urc monomers, being disproportionately located at the dimerization interface. Most residues found at the dimerization interface are conserved or semiconserved between *A. flavus* and *C. utilis*. We speculate that Urc stability, rather than reflecting global electrostatics, is determined by local ionic interactions at the subunit interfaces that are optimal at pH 8. Interfacial ionic bonding is thought to be important to the stability of a number of multimeric enzymes.[41−43]

SEC data showed that inactive Urc aggregates nonspecifically, forming a range of species containing varying numbers of denatured Urc molecules. The rate of aggregation declines at higher pH values as the protein gains more net negative charge, leading to greater intermolecular repulsion between denatured Urc molecules, so we conducted the majority of our studies at pH 10.

Kinetics and Reversibility of Inactivation. All the changes in Urc activity and structure that we observed occur concurrently (Figures 2 and 3), indicating that the major phase of Urc denaturation is a simple two-state transition. These results and other evidence[32,33,44] are consistent with a simple model of inactivation in which disruption at the subunit interfaces, involving destruction of interfacial secondary structure and exposure of interfacial Trp residues to solution, leads to nonspecific aggregation (Figure 1E).

Our studies also show the existence of a relatively rapid reversible phase of Urc denaturation at high temperatures (Figures 3 and 4). An early kinetic-based study of Urc inactivation at ≥58 °C proposed the existence of a rapid transition prior to the predominant kinetic process.[20] A later study, using DSC to assess melting temperatures, identified two separate endotherms. At pH 9.5, these endotherms corresponded to melting temperatures of 49.7 and 60.6 °C;[36] these authors also reported that the lower-temperature process shows some reversibility while the higher-temperature process is irreversible. We suggest that the rapid phase of Urc inactivation observed in this study corresponds to the lower-melting temperature process observed by Bayol et al.,[36] while the slower process, which accounts for the majority of denaturation, corresponds to the higher-temperature process.

Reversibility of denaturation is a function both of the time and of the temperature to which Urc was exposed; it is not simply a function of the degree of inactivation attained (Figure 4). These results indicate that the rapid, reversible phase of Urc denaturation is not coupled with the rest of the denaturation process, because the loss of reversibility is not simply a function of the degree of denaturation.

The presence of DTT during incubation of Urc at elevated temperature decreases the rate of Urc denaturation and increases its reversibility (Figure S5 of the Supporting Information). We find that the irreversibility of the major phase of Urc denaturation arises from aggregation (Figure 1E), so the data in Figure S5 of the Supporting Information suggest that disulfide bond formation contributes to aggregation that can be prevented or reversed in the presence of a reducing agent. The single surface-accessible cysteine group on each monomer is close to the active site and interacts with it (e.g., the presence of the substrate analogue, xanthine, reduces the rate of modification of this cysteine with DTNB[18]), though we observed no change in Urc activity upon assaying in the presence of DTT. Nevertheless, the oxidation state of free Cys residues may affect the stability of the active sites and therefore influence the rate, reversibility, and/or extent of the rapid reversible phase of denaturation. A model in which the rapid reversible phase of Urc inactivation is influenced by the oxidation status of the surface-accessible cysteine residues is consistent with our conclusions and those of others.[18,36]

Glycerol and TMAO Are Urc Stabilizers, but NaCl Destabilizes the Enzyme at Elevated Temperatures. The effect of ionic strength on protein stability in solution is dependent on the balance of attractive and repulsive ionic interactions within the protein, because increasing the ionic strength will lead to increasing the level of screening of these interactions.[40] NaCl has a strong destabilizing effect on Urc at elevated temperatures (Figure 5A and Figure S3 of the Supporting Information), showing that intramolecular ionic interactions stabilize Urc under these conditions. Each

monomer forms six salt bridges with other monomers in the structure of *A. flavus* Urc, with two of these being at the dimerization interface.[45] The model outlined above, in which disruption at the subunit interfaces leads to the observed concurrent changes in structure and activity, is consistent with NaCl-induced destabilization of Urc arising from weakening of favorable intersubunit ionic interactions.

Glycerol stabilizes Urc in a concentration-dependent manner at all temperatures studied (Figures 5B and 6 and Figure S3 of the Supporting Information). Stabilization of proteins by glycerol is due specifically to strengthening of the solvent structure by the polyol. Glycerol, preferentially excluded from the protein surface, enters and reinforces the water lattice structure, so that interactions between protein hydrophobic residues and the solvent become even more energetically unfavorable than contacts with pure water, hence stabilizing hydrophobic interactions within the protein.[46−52] Because partial exposure of hydrophobic residues to the solution is approximately concurrent with Urc inactivation (Figure 2), our results are consistent with this model.

TMAO stabilizes Urc (Figure 5C), though to a lesser degree than glycerol (Figure 5B). TMAO induces helix formation in peptides through the osmophobic effect,[53] and we have shown that loss of ∼20% of the native α-helical structure is concurrent with the inactivation of Urc (Figures 1A and 2). Therefore, our results imply that Urc is stabilized by TMAO through the osmophobic effect, with the additive shifting the equilibrium between native and molten globule states toward the former.[54−56]

We made two observations where the effects of additives were temperature-dependent. The strong destabilizing effect of NaCl on Urc observed at 57.5 and 60.0 °C (Figure 5A and Figure S3 of the Supporting Information) is almost nonexistent at 40.0 °C (Figure 6). In addition, structural studies reveal a contrast between the biophysical changes that occur during inactivation of Urc in the presence of glycerol at 40 °C and those that occur in its presence at 65.0 °C (Figure 7). Therefore, assessing Urc inactivation in the presence of additives at higher temperatures may not give an accurate representation of the slower inactivation process that occurs at lower temperatures; this demonstrates a major limitation of accelerated storage trials, commonly used in the pharmaceutical industry to test shelf life.[57]

As mentioned in the introductory section, attempts to stabilize Urc, through both modification and formulation, have thus far focused on the use of PEG. This study presents the possibility of using other additives to formulate Urc-based pharmaceuticals, specifically those known to have a positive effect on the stability of protein secondary and tertiary structure.

CONCLUSION

This study is, to the best of our knowledge, the first detailed experimental investigation of the structural changes that occur during Urc inactivation. We confirm the existence of a rapid reversible phase of Urc denaturation and show that this phase is not completely coupled with the main phase. Oxidation of a cysteine residue close to the active site may have an effect on the nature of this phase.

The main phase of Urc inactivation involves loss of the majority of tertiary structure and a small proportion of secondary structure, producing molten globules in which there is enhanced surface exposure of Trp residues and that are liable to nonspecific aggregation. This process is summarized in Figure 8. The transition from the native state

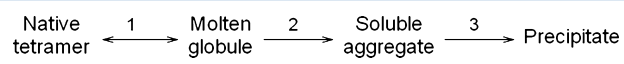

Figure 8. Scheme for the main phase of Urc inactivation. Inactivation leads to the formation of molten globules (step 1) that are prone to aggregation (step 2). The rate of Urc precipitation (step 3) is dependent on the pH of the solution, decreasing with pH over the pH range investigated. The rate of step 1 is also pH-dependent, increasing with pH over the range studied. Step 2 appears to occur almost instantaneously at pH 10, making step 1 practically irreversible.

to the molten globule is possibly initiated by disruption at the subunit interfaces. We show that both glycerol and TMAO stabilize, while NaCl destabilizes, Urc at elevated temperatures, confirming that secondary structure loss, disruption of ionic interactions, and exposure of hydrophobic residues are determinants of the rate of Urc inactivation. Glycerol also stabilizes Urc at lower temperatures and may therefore find application as a formulation component for Urc-based pharmaceuticals. However, we found subtle differences between the effects of additives on Urc inactivation at different temperatures, demonstrating the limitations of using studies at higher temperatures to make predictions about enzyme inactivation under more ambient conditions.

ASSOCIATED CONTENT

Supporting Information

Evidence of the purity of the Urc preparation used, data acquired from SEC and CD experiments with Urc in the presence and absence of DTT, activity data from Urc incubation experiments using buffers of different pH values and from incubations of Urc in NaCl, glycerol, and TMAO formulations conducted at 60 °C, and a graphic representation of the charge distribution in an *A. flavus* Urc monomer to demonstrate the uneven distribution of charged residues in the enzyme. This material is available free of charge via the Internet at http://pubs.acs.org.

AUTHOR INFORMATION

Corresponding Author

*Telephone: +44 (0)1189 989 6940. E-mail: michael.caves@googlemail.com.

Funding

This work was supported by a BBSRC Industrial CASE Studentship (BB/E527763/1) with additional support from Arecor Limited.

Notes

The authors declare no competing financial interest.

ABBREVIATIONS

ANS, 8-anilinonaphthalene-1-sulfonate; CD, circular dichroism; Cys, cysteine; SEC, size exclusion chromatography; Trp, tryptophan; Urc, uricase.

REFERENCES

(1) Holmberg, C. G. (1939) Uricase purification and properties. *Biochem. J. 33*, 1901−1906.

(2) Okumura, I., Kondo, K., Miyake, Y., Itaya, K., and Yamamoto, T. (1976) Stereospecificity of conversion of uric acid into allantoic acid by enzymes of *Canadida utilis*. *J. Biochem. 79*, 1013−1019.

(3) Cammalleri, L., and Malaguarnera, M. (2007) Rasburicase represents a new tool for hyperuricemia in tumor lysis syndrome and in gout. *Int. J. Med. Sci. 4*, 83−93.
(4) Pasut, G., Sergi, M., and Veronese, F. (2008) Anti-cancer PEG-enzymes: 30 years old, but still a current approach. *Adv. Drug Delivery Rev. 60*, 69−78.
(5) Sherman, M., Saifer, M., and Perez-Ruiz, F. (2008) PEG-uricase in the management of treatment-resistant gout and hyperuricemia. *Adv. Drug Delivery Rev. 60*, 59−68.
(6) Chohan, S., and Becker, M. A. (2009) Update on emerging urate-lowering therapies. *Curr. Opin. Rheumatol. 21*, 143−149.
(7) Riley, K. (2010) FDA approves new drug for gout. FDA news release. U.S. Food and Drug Administration (http://www.fda.gov/NewsEvents/Newsroom/PressAnnouncements/ucm225810.htm).
(8) Gochman, N., and Schmitz, J. M. (1971) Automated determination of uric acid, with use of a uricase-peroxidase system. *Clin. Chem. 17*, 1154−1159.
(9) Liao, F., Zhao, Y. S., Zhao, L. N., Tao, J., Zhu, X. Y., and Liu, L. (2006) Evaluation of a kinetic uricase method for serum uric acid assay by predicting background absorbance of uricase reaction solution with an integrated method. *J. Zhejiang Univ., Sci., B 7*, 497−502.
(10) Nakaminami, T., Ito, S., Kuwabata, S., and Yoneyama, H. (1999) Uricase-catalyzed oxidation of uric acid using an artificial electron acceptor and fabrication of amperometric uric acid sensors with use of a redox ladder polymer. *Anal. Chem. 71*, 1928−1934.
(11) Huang, S. H., Shih, Y. C., Wu, C. Y., Yuan, C. J., Yang, Y. S., Li, Y. K., and Wu, T. K. (2004) Detection of serum uric acid using the optical polymeric enzyme biochip system. *Biosens. Bioelectron. 19*, 1627−1633.
(12) Zhao, C., Wan, L., Wang, Q., Liu, S., and Jiao, K. (2009) Highly sensitive and selective uric acid biosensor based on direct electron transfer of hemoglobin-encapsulated chitosan-modified glassy carbon electrode. *Anal. Sci. 25*, 1013−1017.
(13) Chen, D., Wang, Q., Jin, J., Wu, P., Wang, H., Yu, S., Zhang, H., and Cai, C. (2010) Low-potential detection of endogenous and physiological uric acid at uricase-thionine-single-walled carbon nanotube modified electrodes. *Anal. Chem. 82*, 2448−2455.
(14) Bayramoğlu, G., Altıntaş, B., and Arıca, M. Y. (2011) Reversible immobilization of uricase on conductive polyaniline brushes grafted on polyacrylonitrile film. *Bioprocess Biosyst. Eng. 34*, 127−134.
(15) Freitas, Dda. S., Spencer, P., Vassão, R., and Abrahão-Neto, J. (2010) Biochemical and biopharmaceutical properties of PEGylated uricase. *Int. J. Pharm. 387*, 215−222.
(16) Zhang, C., Yang, X., Feng, J., Yuan, Y., Li, X., Bu, Y., Xie, Y., Yuan, H., and Liao, F. (2010) Effects of modification of amino groups with poly(ethylene glycol) on a recombinant uricase from *Bacillus fastidiosus*. *Biosci., Biotechnol., Biochem. 74*, 1298−1301.
(17) Bomalaski, J. S., Holtsberg, F. W., Ensor, C. M., and Clark, M. A. (2002) Uricase formulated with polyethylene glycol (uricase-PEG 20): Biochemical rationale and preclinical studies. *J. Rheumatol. 29*, 1942−1949.
(18) Nishimura, H., Yoshida, K., Yokota, Y., Matsushima, A., and Inada, Y. (1982) Physicochemical properties and states of sulfhydryl groups of uricase from *Candida utilis*. *J. Biochem. 91*, 41−48.
(19) Colloc'h, N., El Hajji, M., Bachet, B., L'Hermite, G., Schiltz, M., Prangé, T., Castro, B., and Mornon, J. (1997) Crystal structure of the protein drug urate oxidase-inhibitor complex at 2.05 Å resolution. *Nat. Struct. Biol. 4*, 947−952.
(20) Pitts, O., Priest, D., and Fish, W. (1974) Uricase. Subunit composition and resistance to denaturants. *Biochemistry 13*, 888−892.
(21) Conley, T. G., and Priest, D. G. (1980) Thermodynamics and stoicheiometry of the binding of substrate analogues to uricase. *Biochem. J. 187*, 727−732.
(22) Retailleau, P., Colloc'h, N., Vivarès, D., Bonneté, F., Castro, B., El-Hajji, M., Mornon, J., Monard, G., and Prangé, T. (2004) Complexed and ligand-free high-resolution structures of urate oxidase (Uox) from *Aspergillus flavus*: A reassignment of the active-site binding mode. *Acta Crystallogr. D60*, 453−462.
(23) Whitmore, L., and Wallace, B. (2004) DICHROWEB, an online server for protein secondary structure analyses from circular dichroism spectroscopic data. *Nucleic Acids Res. 32*, W668−W673.
(24) Hennessey, J. P., Jr., and Johnson, W. C., Jr. (1981) Information content in the circular dichroism of proteins. *Biochemistry 20*, 1085−1094.
(25) Whitmore, L., and Wallace, B. A. (2008) Protein Secondary Structure Analyses from Circular Dichroism Spectroscopy: Methods and Reference Databases. *Biopolymers 89*, 392−400.
(26) Kelly, S., Jess, T., and Price, N. (2005) How to study proteins by circular dichroism. *Biochim. Biophys. Acta 1751*, 119−139.
(27) Barrow, C. J., Yasuda, A., Kenny, P. T., and Zagorski, M. G. (1992) Solution conformations and aggregational properties of synthetic amyloid β-peptides of Alzheimer's disease. Analysis of circular dichroism spectra. *J. Mol. Biol. 225*, 1075−1093.
(28) Coleman, D. L., and Blout, E. R. (1968) The optical activity of the disulfide bond in L-cystine and some derivatives of L-cystine. *J. Am. Chem. Soc. 90*, 2405−2416.
(29) Horwitz, J., Strickland, E. H., and Billups, C. (1969) Analysis of vibrational structure in the near-ultraviolet circular dichroism and absorption spectra of phenylalanine and its derivatives. *J. Am. Chem. Soc. 91*, 184−190.
(30) Dolgikh, D., Gilmanshin, R., Brazhnikov, E., Bychkova, V., Semisotnov, G., Venyaminov, S. Yu., and Ptitsyn, O. (1981) α-Lactalbumin: Compact state with fluctuating tertiary structure? *FEBS Lett. 136*, 311−315.
(31) Stryer, L. (1965) The interaction of a naphthalene dye with apomyoglobin and apohemoglobin. A fluorescent probe of non-polar binding sites. *J. Mol. Biol. 13*, 482−495.
(32) Girard, E., Marchal, S., Perez, J., Finet, S., Kahn, R., Fourme, R., Marassio, G., Dhaussy, A. C., Prangé, T., Giffard, M., Dulin, F., Bonneté, F., Lange, R., Abraini, J. H., Mezouar, M., and Colloc'h, N. (2010) Structure-function perturbation and dissociation of tetrameric urate oxidase by high hydrostatic pressure. *Biophys. J. 98*, 2365−2373.
(33) Liu, Z., Lu, D., Li, J., Chen, W., and Liu, Z. (2009) Strengthening intersubunit hydrogen bonds for enhanced stability of recombinant urate oxidase from *Aspergillus flavus*: Molecular simulations and experimental validation. *Phys. Chem. Chem. Phys. 11*, 333−340.
(34) London, M., and Hudson, P. (1956) Purification and properties of solubilized uricase. *Biochim. Biophys. Acta 21*, 290−298.
(35) Itaya, K., Yamamoto, T., and Fukumoto, J. (1967) Studies on yeast uricase, part I. Purification and some enzymatic properties of yeast uricase. *Agric. Biol. Chem. 31*, 1256−1264.
(36) Bayol, A., Dupin, P., Boe, J. F., Claudy, P., and Létoffé, J. M. (1995) Study of pH and temperature-induced transitions in urate oxidase (Uox-EC1.7.3.3) by microcalorimetry (DSC), size exclusion chromatography (SEC) and enzymatic activity experiments. *Biophys. Chem. 54*, 229−235.
(37) Tan, Q., Wang, N., Yang, H., Zhang, L., Liu, S., Chen, L., Liu, J., Zhang, L., Hu, N., Zhao, C., and Zhang, J. (2010) Characterization, stabilization and activity of uricase loaded in lipid vesicles. *Int. J. Pharm. 384*, 165−172.
(38) Itaya, K., Fukumoto, J., and Yamamoto, T. (1971) Studies on urate oxidase of *Candida utilis*, part II. Some physical and chemical properties of the purified enzyme. *Agric. Biol. Chem. 35*, 813−821.
(39) Liu, J., Li, G., Liu, H., and Zhou, X. (1995) Purification and properties of uricase from *Candida* sp. and its application in uric acid analysis in serum. *Ann. N.Y. Acad. Sci. 750*, 477−481.
(40) Dominy, B. N., Perl, D., Schmid, F. X., and Brooks, C. L., III (2002) The effects of ionic strength on protein stability: The cold shock protein family. *J. Mol. Biol. 319*, 541−554.
(41) Yip, K. S., Stillman, T. J., Britton, K. L., Artymiuk, P. J., Baker, P. J., Sedelnikova, S. E., Engel, P. C., Pasquo, A., Chiarluce, R., and Consalvi, V. (1995) The structure of *Pyrococcus furiosus* glutamate dehydrogenase reveals a key role for ion-pair networks in maintaining enzyme stability at extreme temperatures. *Structure 3*, 1147−1158.
(42) Arnott, M. A., Michael, R. A., Thompson, C. R., Hough, D. W., and Danson, M. J. (2000) Thermostability and thermoactivity of

citrate synthases from the thermophilic and hyperthermophilic archaea, *Thermoplasma acidophilum* and *Pyrococcus furiosus*. *J. Mol. Biol. 304*, 657−668.
(43) Caves, M. S., Derham, B. K., Jezek, J., and Freedman, R. B. (2011) The mechanism of inactivation of glucose oxidase from *Penicillium amagasakiense* under ambient storage conditions. *Enzyme Microb. Technol. 49*, 79−87.
(44) Retailleau, P., Colloc'h, N., Vivarès, D., Bonneté, F., Castro, B., El Hajji, M., and Prangé, T. (2005) Urate oxidase from *Aspergillus flavus*: New crystal-packing contacts in relation to the content of the active site. *Acta Crystallogr. D61*, 218−229.
(45) Colloc'h, N., Girard, E., Dhaussy, A. C., Kahn, R., Ascone, I., Mezouar, M., and Fourme, R. (2006) High pressure macromolecular crystallography: The 140-MPa crystal structure at 2.3 Å resolution of urate oxidase, a 135-kDa tetrameric assembly. *Biochim. Biophys. Acta 1764*, 391−397.
(46) Back, J., Oakenfull, D., and Smith, M. (1979) Increased thermal stability of proteins in the presence of sugars and polyols. *Biochemistry 18*, 5191−5196.
(47) Gekko, K. (1981) Mechanism of polyol-induced protein stabilization: Solubility of amino acids and diglycine in aqueous polyol solutions. *J. Biochem. 90*, 1633−1641.
(48) Gekko, K., and Timasheff, S. N. (1981) Mechanism of protein stabilization by glycerol: Preferential hydration in glycerol-water mixtures. *Biochemistry 20*, 4667−4676.
(49) Gekko, K., and Timasheff, S. N. (1981) Thermodynamic and kinetic examination of protein stabilization by glycerol. *Biochemistry 20*, 4677−4686.
(50) Gekko, K., and Koga, S. (1983) Increased thermal stability of collagen in the presence of sugars and polyols. *J. Biochem. 94*, 199−205.
(51) Gekko, K., and Ito, H. (1990) Competing solvent effects of polyols and guanidine hydrochloride on protein stability. *J. Biochem. 107*, 572−577.
(52) Timasheff, S. (1993) The control of protein stability and association by weak interactions with water: How do solvents affect these processes? *Annu. Rev. Biophys. Biomol. Struct. 22*, 67−97.
(53) Celinski, S., and Scholtz, J. (2002) Osmolyte effects on helix formation in peptides and the stability of coiled-coils. *Protein Sci. 11*, 2048−2051.
(54) Baskakov, I., and Bolen, D. (1998) Forcing thermodynamically unfolded proteins to fold. *J. Biol. Chem. 273*, 4831−4834.
(55) Qu, Y., Bolen, C., and Bolen, D. (1998) Osmolyte-driven contraction of a random coil protein. *Proc. Natl. Acad. Sci. U.S.A. 95*, 9268−9273.
(56) Bolen, D., and Baskakov, I. (2001) The osmophobic effect: Natural selection of a thermodynamic force in protein folding. *J. Mol. Biol. 310*, 955−963.
(57) Waterman, K. C., and Adami, R. C. (2005) Accelerated aging: Prediction of chemical stability of pharmaceuticals. *Int. J. Pharm. 293*, 101−125.